Electronic Supplementary Material (ESI) for Nanoscale.

Supporting Information

Melamine-Assisted One-Pot Synthesis of Hierarchical Nitrogen-Doped Carbon@MoS_2 Nanowall Core-Shell Microspheres and Their Enhanced Li-Storage Performances

Fugen Sun, Yanju Wei, Jianzhuang Chen, Donghui Long, Licheng Ling, Yongsheng Li, Jianlin Shi**

Dr. F. Sun, Dr. J. Chen, Prof. Y. Li, Prof. J. Shi
Lab of Low-Dimensional Materials Chemistry, School of Materials Science and Engineering, China University of Science and Technology, Shanghai 200237, China.

Dr. Y. Wei, Prof. D. Long, Prof. L. Ling
State Key Laboratory of Chemical Engineering, East China University of Science and Technology, Shanghai 200237, China.

Prof. J. Shi
State Key Laboratory of High Performance Ceramics and Superfine Microstructure, Shanghai Institute of Ceramics, Chinese Academy of Sciences, Shanghai 200050, China

*To whom correspondence should be addressed. E-mail: longdh@mail.ecust.edu.cn; jlshi@mail.sic.ac.cn.

Content:

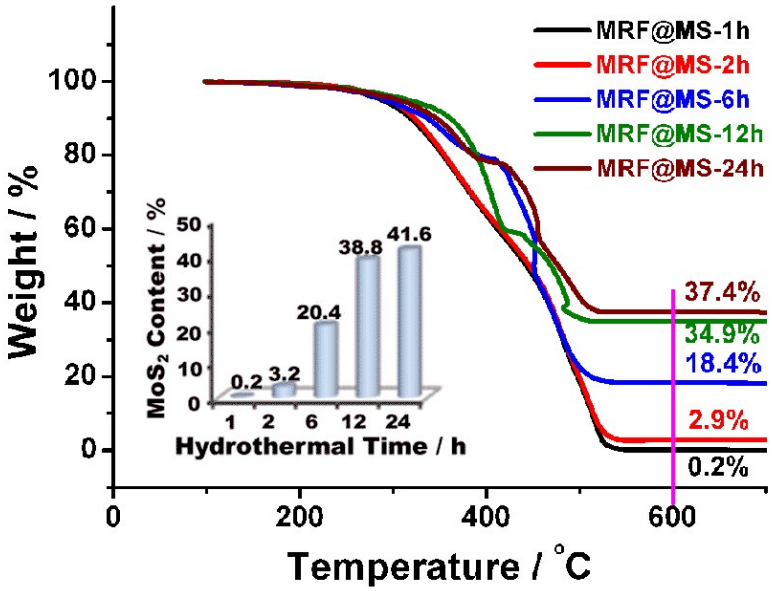

Figure S1. TG analysis in air of as-synthesized MRF@MoS_2 microspheres at different hydrothermal times without heat-treatment (denoted as MRF@MoS_2-xh, where x represents the hydrothermal time). The MRF@MoS_2 microspheres underwent significant weight loss mainly below 550 °C, which can perhaps be attributed to combustion of MRF polymer microspheres, and oxidation of MoS_2 to MoO_3. By assuming that the remaining product after the TGA measurement is MoO_3, the MoS_2 contents in the MRF@MoS_2 microspheres could be calculated, as shown in the inset. After the initial hydrothermal time of 1 h, the collected samples are MRF polymer microspheres and contain almost no MoS_2. After hydrothermal reaction for 2 h, the MRF microsphere surfaces are covered by MoS_2 nuclei nanoparticles with a content of 3.2 wt.%. The MoS_2 contents increase from 20.4 wt.% for MRF@MS-6h composites to 38.8 wt.% for MRF@MS-12h composites and 41.6 wt.% for MRF@MS-24h composites, further confirming the continuous growth of MoS_2 nanowalls during the hydrothermal process.

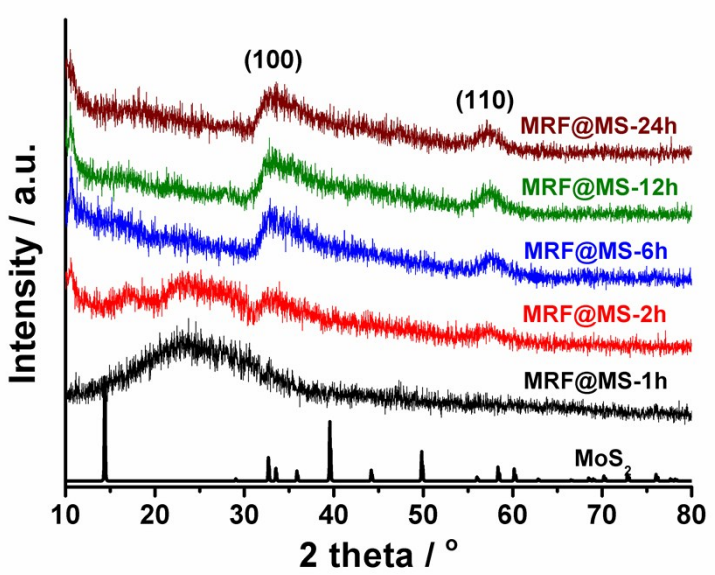

Figure S2. XRD patterns of as-synthesized MRF@MoS_2 microspheres at different hydrothermal times without heat-treatment (denoted as MRF@MoS_2-xh, where x represents the hydrothermal time). No MoS_2 diffraction peaks are present and a wide diffraction peak (2θ) is obviously observed at around 24.2° that corresponds to the pure MRF polymer in the collected samples after hydrothermal reaction for 1 h. After hydrothermal time for 2-24 h, two weak peaks at 32.8° and 57.5° can be found which are respectively attributed to the (100) and (110) crystal planes of typical hexagonal 2H-MoS_2. These results further suggest the direct coverage of MoS_2 on the fast formed MRF polymer microspheres.

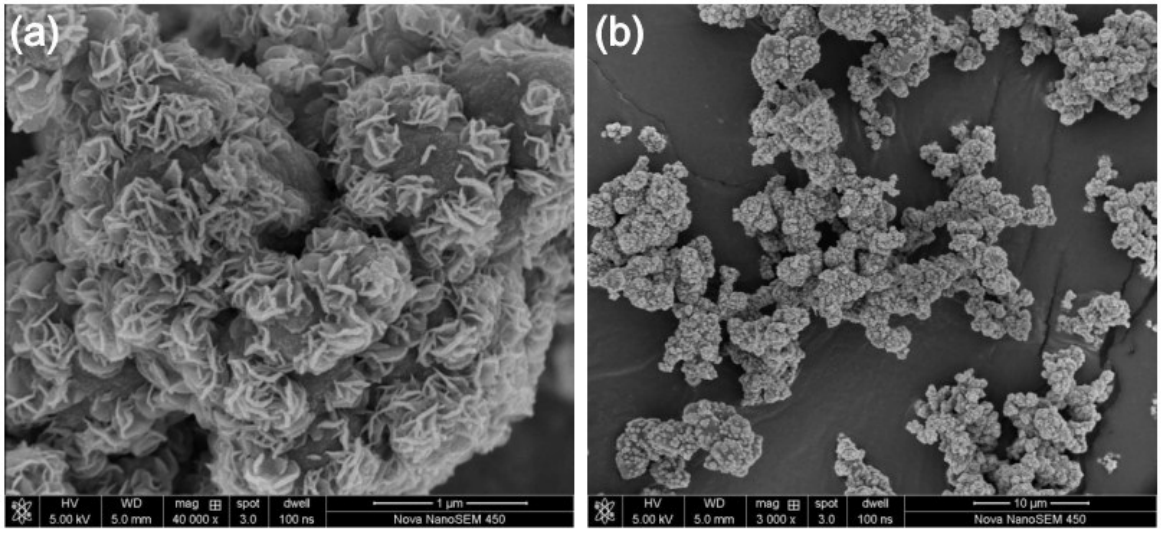

Figure S3. (a) and (b) SEM images of as-synthesized RF/MoS_2 composites without the addition of melamine in the initial hydrothermal precusors. The RF/MoS_2 composites show irregular morphology with a small amount of MoS_2 nanowalls decorated on the RF polymer particles. It is evident that the melamine could be key on the formation of the core-shell microspherical morphology.

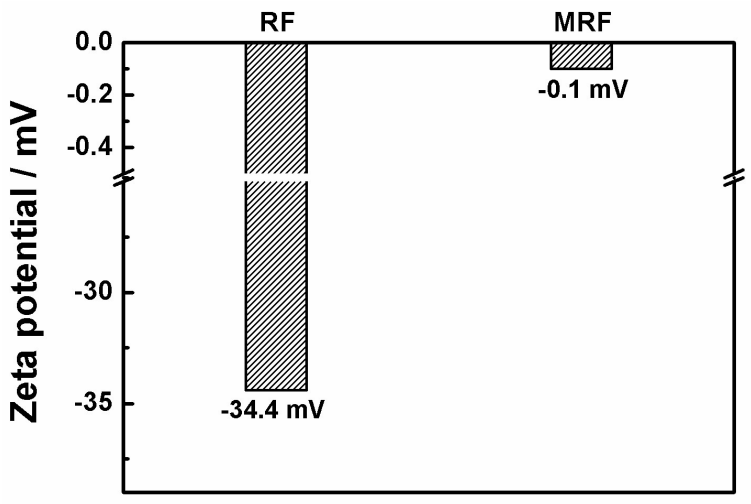

Figure S4. Zeta potential of the RF and MRF colloidal microspheres. The pure RF and MRF polymeric microspheres were prepared through the hydrothermal method without the addition of Na_2MoO_4 and NH_2CSNH_2 as reported in our previous work (H. Zhou, S. Xu, H. Su, et al. *Chem. Commun.*, 2013, **49**, 3763). The RF colloidal microspheres are highly negatively charged with a Zeta potential value of -34.4 mV. The nitrogen functionality inherited from melamine precursor could apparently increase the surface charge of the MRF colloidal microspheres. This increased surface charge of MRF microsphere caused by nitrogen functionality is favorable for the adsorbtion of MoO_4^{2-} anion and subsequent coating of MoS_2 due to the reduced electrostatic repulsion force, which could further inhibit the continuous growth of MRF microspheres.

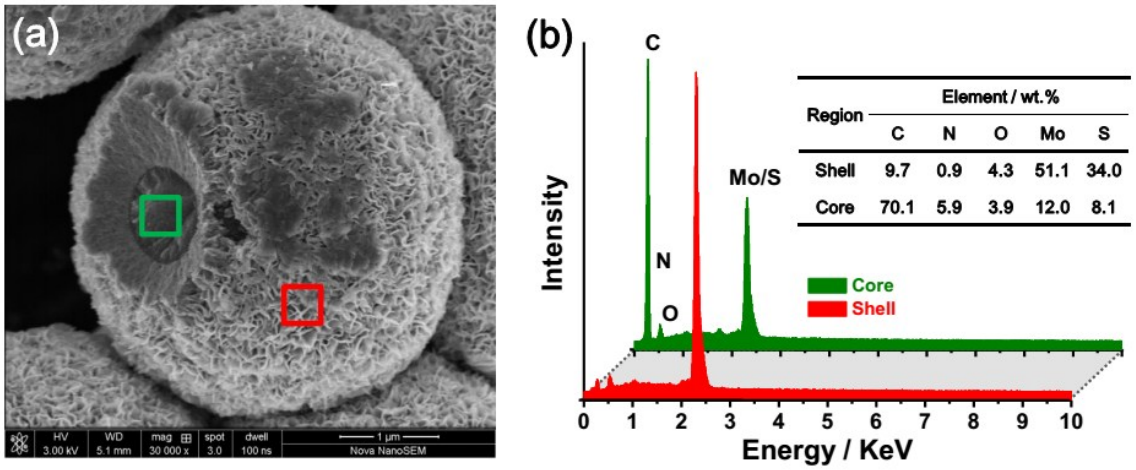

Figure S5. (a) The SEM image of the cracked NC@70MS core-shell microspheres; (b) Elemental EDX analysis of the core region (the red rectangle indication) and the shell region (the green rectangle indication) in (a). The SEM image of the cracked microspheres confirms the cores are in the middle site of the microspheres due to the conformal coverage of the shells. EDX characterizations give the stronger signals of Mo/S in the shell region and the stronger signal of C in the core region respectively. These significant differences further confirm that the NC@MoS_2 microspheres are composed of the carbon cores and the MoS_2 shells. However, due to the semi-quantitative features of the EDX method, the MoS_2 content in the microspheres obtained from EDX analysis is very different from that determined by TGA analysis. Furthermore, it is calculated that the atomic ratio of Mo to S approaches the theoretical value of 1/2, further suggesting the formation of stoichiometric MoS_2.

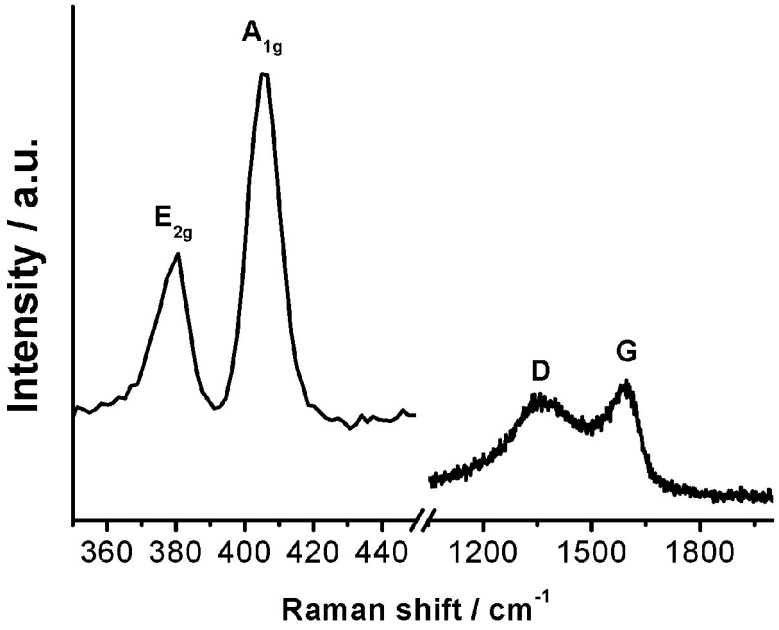

Figure S6. Raman spectra of the NC@70MS core-shell microspheres. The Raman spectra of the NC@70MS core-shell microspheres shows the typic characteristic E_{2g} and A_{1g} bands of MoS_2, located at ca. 380.7 and 406.5 cm^{-1}, respectively. The E_{2g} mode involves the in-layer displacements of Mo and S atoms whereas the A_{1g} mode involves the out-of-layer symmetric displacements of S atoms along the c -axis. The Raman peaks at 1356 cm^{-1} and 1593 cm^{-1} are repectively assigned to the typical characteristic D- and G- bands of disordered graphitic carbon materials.

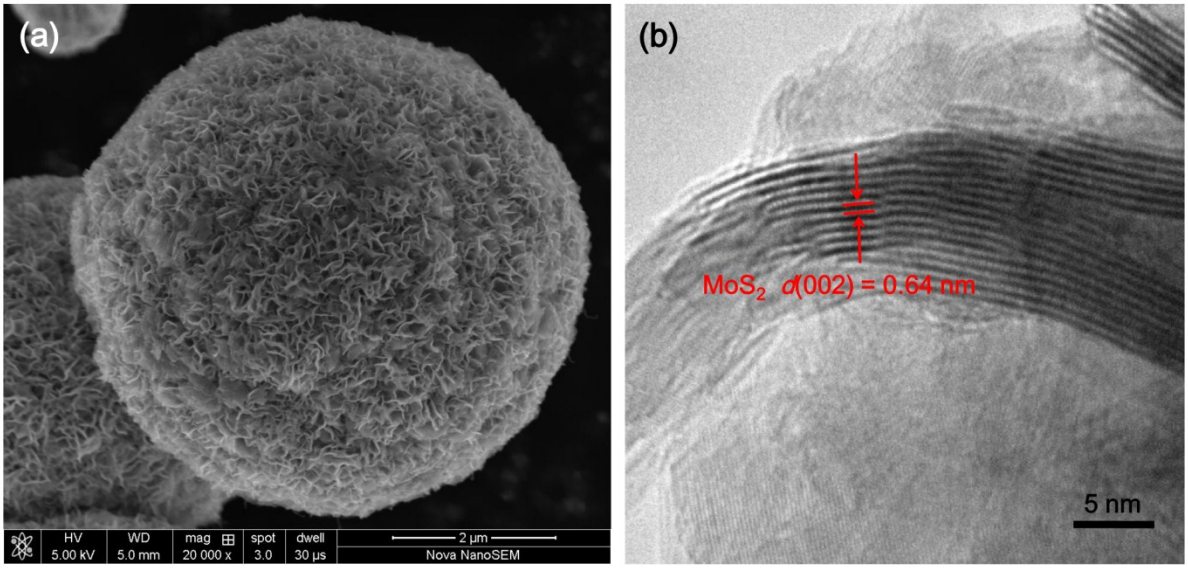

Figure S7. (a) SEM image of the NC@50MS core-shell microspheres and (b) HRTEM image of the MoS_2 nanowalls. The NC@50MS core-shell microspheres have the hierarchical MoS_2 shells constituted of few-layered MoS_2 nanowalls with a similar interlayer spacing as other three samples.

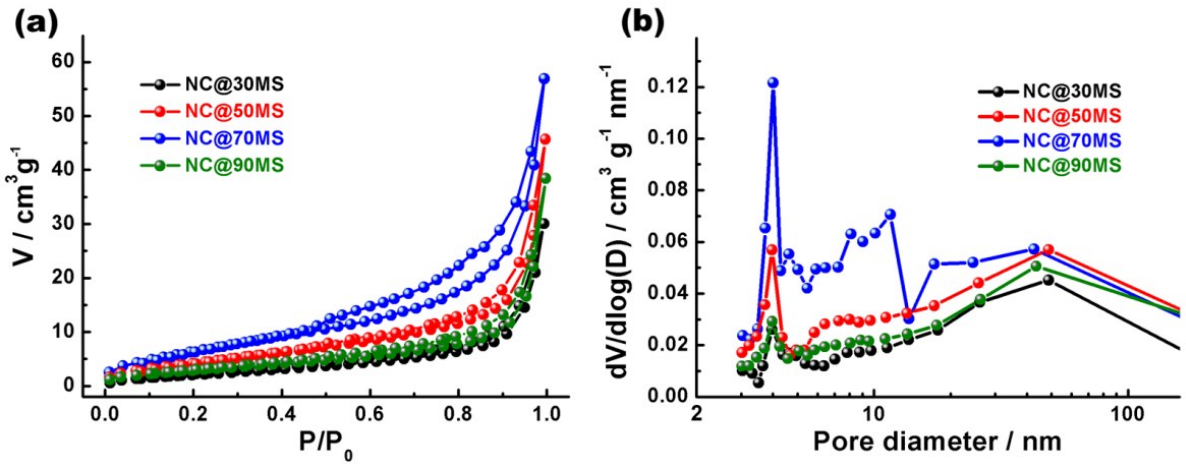

Figure S8. (a) N_2 adsorption-desorption isotherms and (b) BJH pore size distributions of the NC@MoS_2 core-shell microspheres with different MoS_2 contents. All isothermals exhibit the type-IV behaviours with pronounced adsorptions at high relative pressures (0.8-1.0 P/P_0), suggesting that mesopores and macropores coexist in the NC@MoS_2 core-shell microspheres. The mesoporous and macroporous structures are a result of the inter-connection of the ultrathin MoS_2 nanowalls. The NC@70MS core-shell microspheres have a BET surface area of 26 m^2 g^{-1} and a total pore volume of 0.1 cm^3 g^{-1}. The detail pore parameters of the NC@MoS_2 core-shell microspheres with different MoS_2 contents were listed in Table S1. Such hierarchical porous structures could not only faciliate the diffussion of Li-ion, but also accommodate the large volume expansion during the charge-discharge cycles.

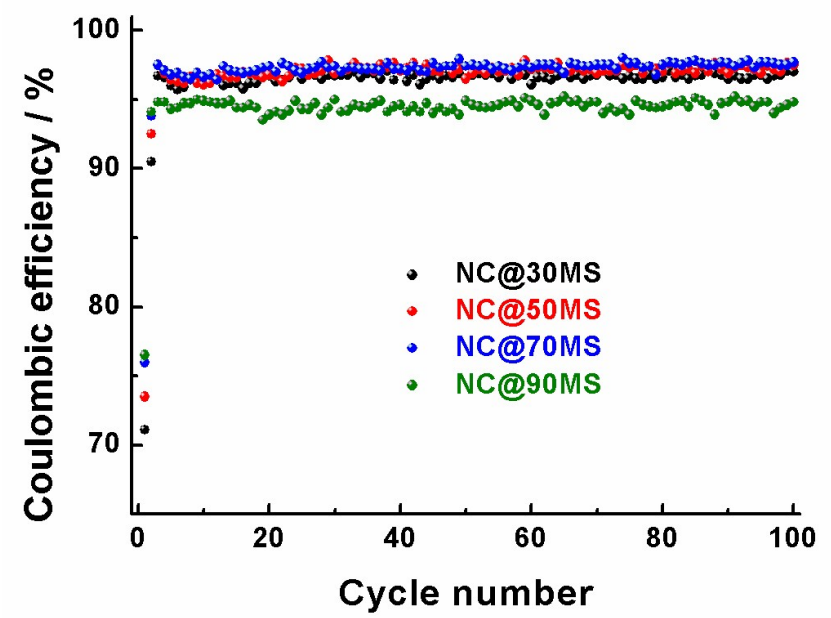

Figure S9. Coulombic efficiency of the NC@MoS_2 core-shell microspheres with different MoS_2 contents. The initial columbic efficiency of the NC@70MS core-shell microspheres is 76%. The initial irreversible capacity loss could be mainly attributed to the formation of the thick gel-like polymeric layer from the electrochemically driven electrolyte degradation, or the trapping of lithium inside the lattice. The coulombic efficiency of the NC@70MS core-shell microspheres increases to 93.8% for the second cycle, 97.5% for the third cycle and 97.7% after 100 cycles, suggesting the excellent structure stability upon cycles. The NC@90MS core-shell microspheres exhibit a lower coulombic efficiency of 94.8% after 100 cycles, possibly due to the significant deterioration of electronic/ionic conductivity caused by the excess MoS_2 coverage.

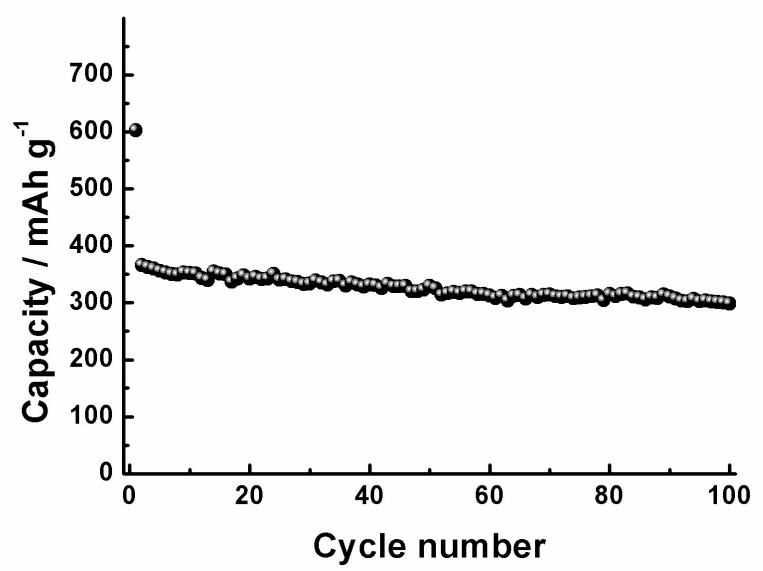

Figure S10. Cycle performance of the nitrigen-doped carbon microspheres (NC) carbonized from the MRF polymer microspheres at a current rate of 100 mA g^{-1}. The specific capacity of NC is 298.9 mAh g^{-1}after 100 cycles, significantly lower than that of MoS_2.

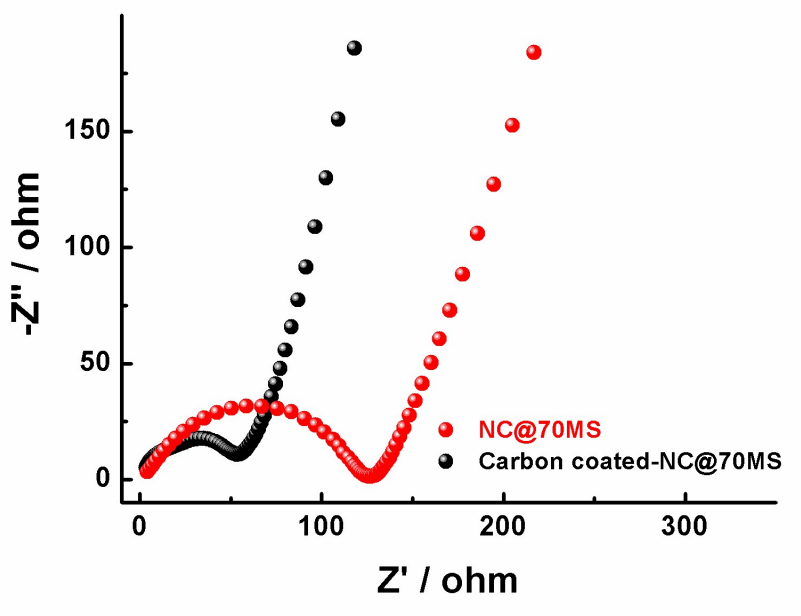

Figure S11. EIS before the first cycle of the NC@70MS core-shell microspheres and the carbon coated-NC@70MS microspheres. The carbon coated-NC@70MS microspheres exhibit faster charge-transfer kinetics than the NC@70MS core-shell microspheres.

Table S1. Pore parameters of the NC@MoS_2 core-shell microspheres with different MoS_2 contents.

Sample	S_{BET} / m^2 g^{-1}	V_t / cm^3 g^{-1}
NC@30MS	9	0.05
NC@50MS	17	0.07
NC@70MS	26	0.09
NC@90MS	12	0.06